

# On the cosmological performance of photometric classified supernovae with machine learning

Marcelo Vargas dos Santos,<sup>1</sup> Miguel Quartin,<sup>1,2</sup> Ribamar R. R. Reis<sup>1,2</sup>

<sup>1</sup>Instituto de Física, Universidade Federal do Rio de Janeiro, 21941-972, Rio de Janeiro, RJ, Brazil

<sup>2</sup>Observatório do Valongo, Universidade Federal do Rio de Janeiro, 20080-090, Rio de Janeiro, RJ, Brazil

25 August 2022

## ABSTRACT

The efficient classification of the different types of Supernova is one of the most important problems of the observational cosmology. Spectroscopic confirmation of most objects in upcoming photometric surveys, such as the Dark Energy Survey and the Large Synoptic Survey Telescope, will be nevertheless impossible. The development of automated classification process based on photometry has thus become a great challenge. In this paper we investigate the performance of machine learning classification on the final cosmological constraints using simulated lightcurves from The Supernova Photometric Classification Challenge, released in 2010. We study the use of different feature sets for the lightcurves and many different ML pipelines based on either decision tree ensembles or automated search processes. To construct the final catalogs we propose a threshold selection method, by employing a *Bias-Variance tradeoff*. This is a very robust and efficient way to minimize the Mean Squared Error. With it we were able to get very strong cosmological performance, which was able to keep  $\sim 75\%$  of the total information in the type Ia SNe in the case of the SALT2 feature set and  $\sim 33\%$  in the case of other feature sets (based on either the Newling model or on standard wavelet decomposition).

**Key words:** supernovae, machine learning, cosmology, photometric classification

## 1 INTRODUCTION

Current and next generation optical surveys which cover large areas with good cadence, like the Dark Energy Survey (DES, Abbott et al. 2016), the Large Synoptic Survey Telescope (LSST, Abell et al. 2009) and the Zwicky Transient Facility (ZTF, Bellm 2014) will not provide spectra of the majority of observed objects. This has pushed the community to develop tools which optimize the amount of science that can be gained from the purely photometric data. Most effort has been focused on how to determine the redshift (see, for instance, Abdalla et al. (2011); Dahlen et al. (2013); Sadeh et al. (2016); Gomes et al. (2018) and references therein). For the cosmological use of supernovae (SNe), determining the redshift is not enough, as it is crucial to correctly classify them in order to isolate the type Ia SNe (which are standardizable candles) from all other types, which are core-collapse SN and that have so far not been proved to be usable as distance indicators (Ishida 2019).

For the flat  $w$ CDM cosmological model, in which dark energy has a constant equation of state, taking into account all systematic uncertainties SN alone is able to constrain  $\Omega_{m0}$  and  $w$  to within 23% and 20%, respectively Scolnic et al. (2018). And since SN data has different parameter degeneracies than CMB and BAO, these uncertainties get much smaller when combining these datasets. A proper classification and redshift determination of future type Ia SN would allow for unprecedented tests on the  $\Lambda$ CDM model as

the number of events would grow from the current number of  $\sim 10^3$  (Betoule et al. 2014; Scolnic et al. 2018) to over  $\sim 10^6$  (Abell et al. 2009).

Such an increase in statistics opens up many new avenues for SN data exploration beyond the conventional Hubble-Lemaître diagram. For instance one can directly measure: anisotropies in the Hubble diagram Koivisto et al. (2011); Colin et al. (2011); Soltis et al. (2019); the Hubble constant for SN in nearby galaxies Riess et al. (2016); Burns et al. (2018); the non-Gaussianities in the scatter of the Hubble diagram due to lensing Quartin et al. (2014); Castro & Quartin (2014); Macaulay et al. (2017); the correlations in the same scatter induced by the peculiar velocities of the SN Gordon et al. (2007); Castro et al. (2016); Howlett et al. (2017); Garcia et al. (2019); and the time-delays in multiply-imaged SNe Oguri & Marshall (2010); Bonvin et al. (2017); Birrer et al. (2019); Huber et al. (2019).

The SN classification scheme does not need to be boolean. Instead techniques have been proposed in Kunz et al. (2007); Newling et al. (2012) to make use of SN catalogs for which each event has a set of probabilities of belonging to different types. Nevertheless, the higher the classification probability of each object, the better these kind of techniques can work. Current SN catalogs have employed a SN classification scheme based on an empirical template fitting Sako et al. (2018); Jones et al. (2018). But in recent years alternative classifications scheme have been proposed Ishida

arXiv:1908.04210v1 [astro-ph.CO] 12 Aug 2019

& de Souza (2013) and a couple of large classification challenges have been held Kessler et al. (2010a); Malz et al. (2018). In particular, the use of machine learning (ML) techniques in SN classification is starting to be studied in more detail Charnock & Moss (2017); Lochner et al. (2016); Moss (2018).

The historical standard technique to perform photometric classification is through template matching. It consists in constructing the photometric light curves as a combination, linear or otherwise, of spectra from a template set, and comparing it with the real one. The coefficients are then determined performing a numerical optimization (say, by a  $\chi^2$  minimization): see for instance Sako et al. (2018). This is still the most common technique in Supernovae Surveys, and form the basis of SN compilations such as the SDSS-II Kessler et al. (2009), JLA Betoule et al. (2014) and Pantheon Scolnic et al. (2018) catalogs. In this decade some groups started to use Machine Learning techniques to improve this classification. In SDSS-II the authors applied the Nearest Neighbors (NN) algorithm to see if it could improve their Photometric SN Identification (PSNID) template fitting software Sako et al. (2018). The Pan-STARRS team compared the NN with 3 different template fitting codes: PSNID, GalSNID and Fitprob. Recently Villar et al. (2019) employed machine learning methods to classify photometrically Pan-STARRS supernovae. The first public release of the `scikit-learn`<sup>1</sup> Pedregosa et al. (2011) library in 2010 increased the popularity of the ML methods as it provides many sophisticated and complex machine learning models in a very simple implementation. It made easy for anyone to write efficient codes with few lines. Training a model and making predictions are easily carried out using intuitive commands like `fit` and `predict`. In (Lochner et al. 2016) (henceforth **L16**) the authors performed the first thorough comparison between many `scikit-learn` models (including the NN) and found that a boost method of decision trees ensemble, the AdaBoost classifier, reached the best AUC score, which is the area under the *Receiver Operating Characteristic* curve (see below).

In this work we use the simulations performed as part of the Supernova Photometric Classification Challenge (SNPCC), discussed below in Section 3, in order to perform our ML training and tests. We start by performing a comparison similar to **L16** but expanding to other ensemble Decision Trees provided by `scikit-learn`: Adaptive Boosting (**ADA**), RandomForest (**RF**), ExtraTrees (**EXT**), Gradient Boosting (**GB**), and the Extreme Gradient Boosting (**XGB**) provided by the `XGBoost` library<sup>2</sup> and testing also an alternative metric to characterize the performance of the classifier: the *Average Purity* (AP), while **L16** used only the AUC, which is the area under the Receiver Operating Characteristic (ROC) curve. We also performed an automated machine learning training by using TPOT,<sup>3</sup> in this way we found the best pipelines for each feature set, **L16** used a simple pipeline for all cases, a `StandardScaler` transform followed by the machine learning model. We then explore how a ML-classified SN catalog performs in cosmological parameter estimation, quantifying the degradation due to the imperfect completeness and purity of the resulting catalogs. These results should be directly applicable to the SN in DES due to the similar numbers of both SN with only photometry and of SN with spectra that can be used to train the algorithm.

This paper is structured as follows: in section 2 we summa-

rize the SNPCC and its specifications; in section 3 we revise the supervised learning approach paying special attention to the *Bias-Variance tradeoff* method 3.1, with more details on decision trees 3.2 and automated machine learning 3.3; in section 4 discuss the different features sets. Finally we present our results and discuss them in section 5 and the conclusions in 6.

## 2 LARGE PHOTOMETRIC SURVEYS AND THE SUPERNOVA PHOTOMETRIC CLASSIFICATION CHALLENGE

One of the greatest challenges in photometry is to infer values of observable quantities which are traditionally computed from spectra. The most recurrent example is the photometric determination of galaxy redshifts. In this work we focus instead solely on a separate photometric problem: supernova classification. While the different SN types are defined by the presence of specific absorption lines, photometric classification must rely instead on their different lightcurve shapes and colors.

The Supernova Photometric Classification Challenge (SNPCC) was proposed by (Kessler et al. 2010a) in order to stimulate the development of tools to address this problem. They have publicly released a blinded mix of simulated SNe, with the different types selected in proportion to their expected rate and in the *griz* filters of the DES with realistic observing conditions (sky noise, point spread function and atmospheric transparency) based on years of recorded conditions at the DES site. Simulations of non-Ia type SNe are based on spectroscopically confirmed light curves that include non-Ia samples donated from the Carnegie Supernova Project (CSP), the Supernova Legacy Survey (SNLS), and the Sloan Digital Sky Survey-II (SDSS-II).

The SNPCC catalog contains 21319 supernovae light curves corresponding to five seasons of observation, simulated by the SNANA software. This set is composed by 5086 type Ia SN, generated by SALT2 and MLCS2k2 models, and 16231 core collapse SN, separated among 7 different types: II, IIn, Iip, IIL, Ib, Ib/c and Ic. The type Ia supernovae were simulated using an equal mix of the models MLCS Jha et al. (2007) and SALT2 Guy et al. (2007) with an additional random color variation. An extinction correction, MLCS-U2 was used in order to make the models agree in the ultraviolet Kessler et al. (2009). The non-Ia supernovae light curves were based on spectroscopically confirmed observed ones and constructed by warping a standard spectral template to match the photometry, and The SN rates were based on the results from Dilday et al. (2008) and Bazin et al. (2009). Ten groups addressed the challenge using different algorithms including template matching and ML techniques. The results of the challenge were published in Kessler et al. (2010a): the template matching code PSNID from Sako et al. (2008) was found to be the best one based on efficiency, purity and completeness.

Since the end of the SNPCC the catalog has been unblinded, and thus provide a very useful tool to train and test ML algorithms which rely on supervised training, in which a subset of the data has known classification *a priori*. In our case in particular this corresponds to assuming we will have a subset of the SN observed spectroscopically.

<sup>1</sup> [scikit-learn.org](https://scikit-learn.org)

<sup>2</sup> [xgboost.ai](https://xgboost.ai)

<sup>3</sup> [epistasislab.github.io/tpot](https://epistasislab.github.io/tpot)

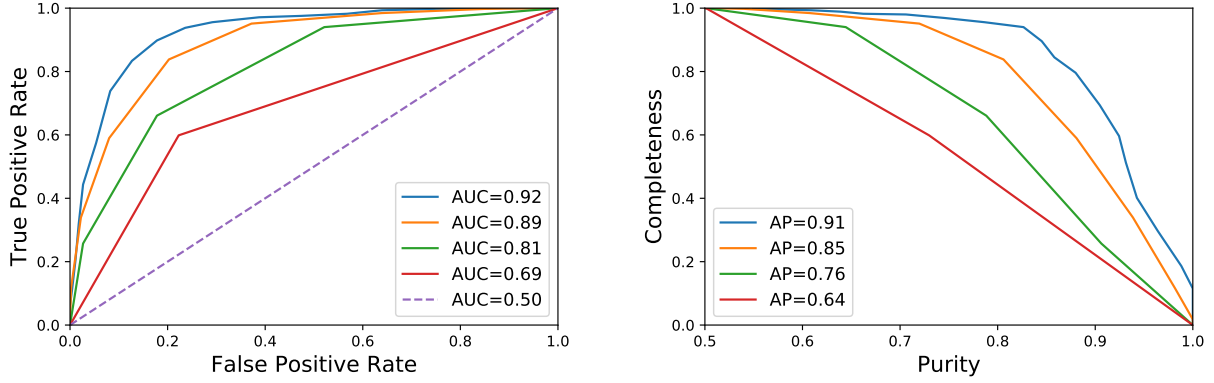


Figure 1. Examples of ROC (left) and *Completeness-Purity* (right) curves.

### 3 THE SUPERVISED MACHINE LEARNING APPROACH

The objective of a supervised learning algorithm is to construct rules, according a method, which relate a set of feature (observable) variables to a target one. These rules can not be so simple, *underfitting*, which returns non realistic predictions; and not so complex, *overfitting*, which can reproduce particular issues only present in the training set data. The balance is set choosing values for the hyper parameters (parameters of the model) which optimize a score function. For a linear model, for instance, the hyperparameters are the intercept and the slope, set to minimize the mean squared error.

In classification problems, like the Supernovae classification, the target variables are classes, represented by integer numbers. In this work we are interested in the cosmological use of type Ia SNe so we consider only two classes: Type Ia (Ia), the positive class (1); and Core Collapse (CC) supernovae, the negative class (0). The output of a classification is the probability of an input correspond to a positive class, Type Ia in our case.

The efficiency of a classifier is completely summarized by four quantities: (i) The number of true positives (TP), i.e. the positive values which were correctly classified; (ii) The number of true negatives (TN), i.e. the negative values which were correctly classified; (iii) The number of false positives (FP), i.e. the positive values which were not correctly classified; (iv) The number of false negatives (FN), i.e. the negative values which were not correctly classified. These are the components of the confusion matrix, shown in Table 1.

All these quantities vary with the probability threshold, but always respecting the bound

$$TP + FP + TN + FN = N, \quad (1)$$

where  $N$  is the length of the data set. So we must choose a value that maximizes the true predictions (TP and TN) and minimizes the false predictions (FP and FN). However we are not sure that the best threshold found in training process is the best for predictions, to avoid this problem we choose a score function, for optimization process, which depends of all threshold values (between 0 and 1). The scores functions are derived from confusion matrix, and in this work we use the area under the *receiver operating characteristic* curve score, the same used in L16, and the Average Precision. To define these scores we must start defining other three quantities:

*Completeness* ( $\mathcal{C}$ ) or *True Positive Rate* (TPR): The fraction of real positives, which are correctly classified, used in final set. Also referred sometimes in the ML literature just as “recall” or

	True Class	
	P	N
Predicted class	True positive (TP)	False positive (FP)
	False negative (FN)	True negative (TN)

Table 1. Confusion matrix for a boolean classification problem.

“sensitivity”, is given by

$$\mathcal{C} = \text{TPR} = \frac{TP}{TP + FN}. \quad (2)$$

*False Positive Rate* (FPR): The fraction of real negatives which are not correctly classified, which contaminate the final set. Also referred as false alarm rate, is given by

$$\text{FPR} = \frac{FP}{FP + TN}. \quad (3)$$

*Purity* ( $\mathcal{P}$ ): The fraction of real positives in the final set. Sometimes referred to in the ML literature as just “precision”, is given by

$$\mathcal{P} = \frac{TP}{TP + FP}. \quad (4)$$

With the above definitions we may define the aforementioned scores.

*Area Under the ROC Curve* (AUC): Both TPR and FPR are, by definition, quantities between 0 and 1. They are used to construct the Receiver Operating Characteristic (ROC) curve, which is just a plot of TPR versus FPR, and is used as a metric for evaluating the performance of classification algorithms. A perfect classifier has  $\text{TPR} = 1$  for any value of FPR, which corresponds to a square of unity area. Imperfect classifiers typically have monotonically increasing ROC curves, which often tend to zero in the limit in which FPR goes to zero and the area under this curve is naturally less than one, as shown in Figure 1. Therefore we define the area under this curve as our score function.

*Average Purity* (AP): Similarly we may define other curve as the plot of *Purity* versus *Completeness*, this curve is know as *Completeness-Purity* (Markel & Bayless 2019; Kgoadi et al. 2019; Villar et al. 2019). In contrast with the ROC, this curve is monotonically decreasing and the purity has a minimum value where

$$\mathcal{P}_{\min} \gtrsim \frac{TP + FP}{TP + FP + TN + FN}, \quad (5)$$

as shown in Figure 1.

For a perfect classifier, the *Purity* is always equal to one for any *Completeness* value, the graph corresponds to the unity square, similar to ROC curve. However the area under this curve is not a reliable score thanks to the numerical noise. To avoid this problem we use the *Average Purity* score (dubbed Average Precision on `scikit-learn` and many ML references)

$$AP = \sum_n (\mathcal{C}_n - \mathcal{C}_{n-1}) \mathcal{P}_n, \quad (6)$$

where the summation is over the thresholds.

Typically a ML problem consists in constructing an optimized pipeline of numerical preprocessing and machine learning methods which could give the best scores, where the score function is chosen according to the problem. As mentioned above, in this work we test the overall classification performance of optimizing one of two different score functions. The first, which follows the SNPCC approach, is the AUC – see also [Swets et al. \(2000\)](#); [Fawcett \(2004\)](#) for accessible discussions on the subject. Since this metric is one of many which can be derived from the confusion matrix, we explore an alternative metric as well, which relies on the area under the curve of completeness versus purity. This is motivated by the fact that in Astronomy one is usually more interested in high-purity catalogs. And since purity is not a linear combination of TPR and FPR, a code that maximizes this AP will not necessarily maximize the AUC.

The optimization process is a random search, drawing 30 points in the hyperparameter space for 200 different training sets, of 1100 objects each, to compute the scores and for 10,000 different training sets to construct the catalogs. The function to perform this kind of search is the `RandomizedSearchCV`, available in `Scikit-Learn`, this function also performs as cross validation split, for which we used the 5-fold split as also used by [L16](#). The cross validation consists, during the training, in split the training set in n-folds, one of these folds is separated, know as validation set, and the model is trained on the remaining folds and the score is computed on the validation set. This step is repeated n times, for each fold, this method is very important to avoid overfitting.

### 3.1 The Bias-Variance tradeoff

We define the bias as the average displacement of the estimated distance modulus from the fiducial value,  $\Delta\mu = \bar{\mu} - \bar{\mu}^{\text{fid}}$ , and the Mean Squared Error (MSE) as the average squared displacement:

$$\text{bias} = \langle \Delta\mu \rangle, \quad \text{MSE} = \langle \Delta\mu^2 \rangle. \quad (7)$$

We will also make use of the Root Mean Squared Error (RMSE) throughout the text. Note that there is a difference between two averages: the one denoted by a bar on the quantity (such as  $\bar{\mu}$ ) represents the mean in a given bin of a given catalog, while the average denoted by  $\langle \dots \rangle$  which represents the ensemble average over the 10,000 catalogs. Using the definition of variance

$$\text{Var}[\Delta\mu] = \langle \Delta\mu^2 \rangle - \langle \Delta\mu \rangle^2 = \text{MSE} - \text{Bias}^2, \quad (8)$$

we find the relation between these quantities

$$\text{MSE} = \text{Var} + \text{Bias}^2. \quad (9)$$

In general the relation between variance and bias is a kind of exchange, i.e. when we change the model hyperparameters in order to decrease one the other increases. The Bias-Variance tradeoff consists in determining which hyperparameters values minimize the

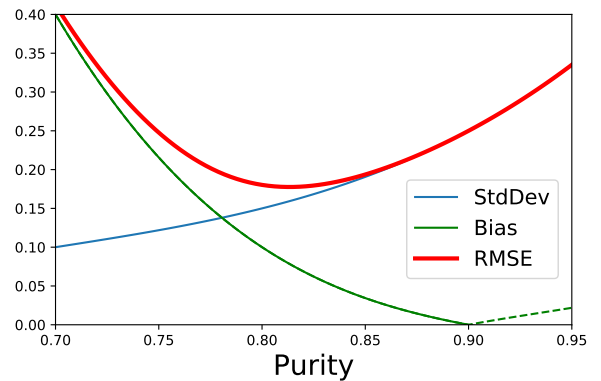


**Figure 2.** Example of how the *Bias-Variance tradeoff* works. The minimum of RMSE (red) depends on the balance between bias (blue) and standard deviation (green).

MSE. The typical *Bias-Variance tradeoff*, as presented in most textbooks and tutorials, is enunciated for regression problems, where the balance between the variance and bias depends on the model complexity. However, in this work since we investigated how a classification problem affects the cosmological distance estimator, the tradeoff depends on the probability threshold, which can be mapped on the purity of the catalog, as shown in Figure 2.

We use the SALT2 as distance estimator, in which the distance modulus for a single supernovae is given by

$$\mu = m_B^* + \alpha x_1 - \beta c - M_B. \quad (10)$$

We assume throughout this simple fiducial model:  $\Lambda$ CDM with  $\Omega_{m0} = 0.3$  and  $H_0 = 70 \text{ km}/(\text{sMpc})$ . We fix the parameters to the fiducial values:  $\alpha = 0.11$ ,  $\beta = 3.2$ .  $M_B$  in principle should also be a constant (which is the basis of assuming SNeIa are standard candles). However, the SNPCC catalog was not generated using only the SALT2 model, and the result is that the SNeIa do not correspond precisely to a given  $\Lambda$ CDM cosmology with a fixed  $M_B$  value. Instead, they exhibit different bestfit  $M_B$  values for different redshifts even assuming the same fiducial cosmology. To simplify our analysis, instead of reproducing the mixed SALT2 / MLCS2k2 model used in the SNPCC, we instead use only the SALT2 model and simply fit for every redshift bin a different value for  $M_B$  in order to enforce  $\Delta\mu_{Ia} = \Delta\mu_{\text{TP}} + \Delta\mu_{\text{FN}} \equiv 0$ . This is enough to make all supernovae equivalent to SALT2 supernovae in the fiducial cosmology above.

### 3.2 Decision trees and ensembles

The first approach that we have investigated is the ensemble of decision trees. The decision tree method consists in constructing a decision flow structure, known as tree, which splits the feature space in a rectangular grid. Each grid cell is then associated with a class (although a given class may end up mapped into various cells). Figure 3 shows an example of a small decision tree for the SALT2 feature set. The main parameters of a typical tree are the maximal depth and the minimum sample per leaf. The leaf is the final node, and which returns a class).

An ensemble of trees is a combination of many different trees, randomly trained. These methods are very useful for analysis of light curves, and some of them were already investigated in recent papers ([Lochner et al. 2016](#); [Markel & Bayless 2019](#); [Kgoadi et al.](#)

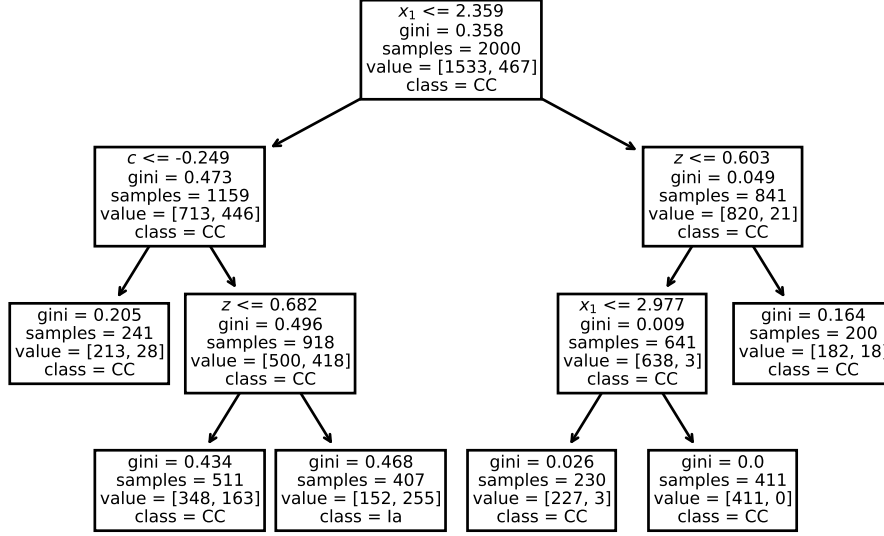


**Figure 3.** Example of a decision tree generated by the `DecisionTreeClassifier`, function from `Scikit-Learn` library, trained on a 2000 sample using the SALT2 feature set.

2019; Villar et al. 2019). In this work we perform a broad comparison between five different ensemble methods. There are two different ways to build an ensemble of decision trees:

1. *Averaging Methods*: the driving principle is to build several independent weak estimators and then use the average of their predictions as the final prediction. On average, the ensemble estimator is usually better than any single estimator because its variance is reduced. In this work we use:

- i Random Forest (**RF**), which constructs a distribution for the classes of the individual trees and take the mode of that as the final class.
- ii Extremely Randomized Trees or Extra-Trees (**EXT**), which combines a special kind of Decision Tree, known as Extra-Tree, that differs from classic decision trees in the way they are built. Thresholds are sorted by choice for each candidate feature and the best is used as the splitting rule.

2. *Boosting Methods*: weak estimators, typically slightly better than a completely random choice, are built sequentially and one tries to reduce the bias of the combined estimator. In this work we used three different boost methods:

- i Adaptive Boost, or AdaBoost (**ADA**), which is a weighted average of the individual predictions, from weak learners, where the weights are computed iteratively.
- ii Gradient Boost (**GB**), which uses the gradient descent method to minimize the loss function.
- iii Extreme Gradient Boost (**XGB**), which is an optimized implementation of the **GB** available in `xgboost.ai`.

### 3.3 Automated Machine Learning

The automated Machine Learning approach aims to determine what is the best pipeline to train the machine learning model by an automated process, i.e. a code that can test several pipelines and assess which one is the best for the problem. The TPOT uses the evolutionary computation framework provided by the DEAP (Distributed

Evolutionary Algorithms in Python)<sup>4</sup> library to choose the best machine learning pipeline.

A typical TPOT pipeline is composed by three main steps: (i) a combination of one or more transformed features copies; (ii) a recursive feature elimination; and (iii) a classifier (or a regressor), which could be a single method or a stacking of many.

One of the most simple pipelines in our work was found when we optimized a classifier for Karpenka features, with AUC as metric:

```

GradientBoostingClassifier(
    learning_rate=0.1, max_depth=8,
    max_features=0.85, min_samples_leaf=4,
    min_samples_split=11, n_estimators=100,
    subsample=0.9
)
    
```

This means that steps (i) and (ii) are reduced to the identity, and (iii) becomes a single `GradientBoostingClassifier`. But when we include the  $z_{\text{host}}$  as a new feature we find a completely different pipeline<sup>5</sup>:

```

make_union(
    FunctionTransformer(copy),
    make_pipeline(
        VarianceThreshold(threshold=0.2),
        FastICA(tol=0.0)
    )
),
XGBClassifier(
    learning_rate=0.1, max_depth=9,
    min_child_weight=2, n_estimators=100,
    nthread=1, subsample=0.8
)
    
```

Step (i) is now to take two copies of the input data and transform one applying a `VarianceThreshold` and `FastICA` in this

<sup>4</sup> [deap.readthedocs.io](http://deap.readthedocs.io)

<sup>5</sup> That is ready to use as argument of the function `sklearn.pipeline.make_pipeline`

Parameter	Range
$z$	(0.01, 1.5)
$t_0$	(-60, 100)
$x_0$	( $-10^{-3}$ , $10^{-3}$ )
$x_1$	(-3, 3)
$c$	(-0.5, 0.5)

**Table 2.** Uniform prior ranges on the SALT2 model parameters.

order, step (ii) is a union of these two copies and (iii) is a XGBClassifier.

## 4 FEATURES EXTRACTION

### 4.1 Template fitting

The template fitting<sup>6</sup> approach consists in reconstruct the light curve of a type Ia supernova, based on templates constructed from previous data sets of type Ia supernovae confirmed by spectroscopy surveys. We fit the light curves computing the flux of the SALT2 model by using the implementation provided by the `sncosmo` library ([sncosmo.readthedocs.io](https://github.com/sncosmo/readthedocs.io)), and sample 1000 points using the multinest method provided by the `PyMultiNest`<sup>7</sup> python library.

In SALT2, the rest-frame specific flux at wavelength  $\lambda$  and phase (time)  $p$  is modeled by ( $p = 0$  at  $B$ -band maximum)

$$\phi(p, \lambda; x_0, x_1, c) = x_0[M_0(t, \lambda) + x_1M_1(t, \lambda)]\exp[cCL(\lambda)], \quad (11)$$

where  $M_0(t, \lambda)$  is average spectral sequence (using past supernova data, [Guy et al. \(2007\)](#)), and  $M_k(t, \lambda)$ ,  $k > 0$ , are higher order components related to the supernova variability (terms with  $k > 1$  are negligible). Finally,  $CL(\lambda)$  is the average color correction.

To compare with photometric SNe Ia data, the observer-frame flux in passband  $Y$  is calculated as

$$F^Y(p(1+z)) = (1+z) \int d\lambda' [\lambda' \phi(p, \lambda') T^Y(\lambda'(1+z))], \quad (12)$$

where  $T^Y(\lambda)$  defines the transmission curve of the observer-frame filter  $Y$ , and  $z$  is the redshift. The free parameters to be fitted are  $x_0$ ,  $x_1$  and  $c$  which are the SED sequence normalization, the stretch and the color parameters respectively, also the  $t_0$  and the supernova redshift,  $z$ . Giving a total of 5 free parameters, for which we use the range of the priors are in 4.1. In addition to the uniform prior for the redshift, we also use the host galaxy redshift  $z_{\text{host}}$ , without changing the ranges of the other parameters.

### 4.2 Parametric models

This approach consists in fitting a functional shape for the light curves for each filter. The advantage over the previous method is that we make less prior assumptions about supernovae. In this work we use the fitted parameters as features for our machine learning algorithms. To fit the light curves we use two models proposed for the SNPCC [Kessler et al. \(2010a,b\)](#): (a) Newling model [Newling et al.](#)

<sup>6</sup> Note that *Template Fitting* refers to methods which use templates of Type Ia light curves to fit other light curves, while *Template Matching* refers to ones which use templates of different types to classify any light curve.

<sup>7</sup> <https://github.com/JohannesBuchner/PyMultiNest>

Parameter	Range
$\log(A)$	(0, 10)
$\phi$	(-60, 100)
$\log(\sigma)$	(-3, 4)
$\log(k)$	(-4, 4)
$\log(\psi)$	(-6, 10)

**Table 3.** Uniform prior ranges on the Newling model parameters.

Parameter	Range
$\log(A)$	( $10^{-3}$ , $10^3$ )
$\log(B)$	( $10^{-3}$ , $10^2$ )
$t_0$	(0, 100)
$t_1$	(0, 100)
$T_{\text{rise}}$	(0, 100)
$T_{\text{fall}}$	(0, 100)

**Table 4.** Uniform prior ranges on the Karpenka model parameters.

(2010); (b) Karpenka model [Karpenka et al. \(2013\)](#). The parameters were determined by sampling 1000 points with the `PyMultiNest` library, as in the previous case.

#### 4.2.1 Newling model

The function form proposed by the Newling model is given by

$$F(t) = A \left( \frac{t - \phi}{\sigma} \right)^k \exp \left( -\frac{t - \phi}{\sigma} \right) k^{-k} e^k + \Psi(t), \quad (13)$$

where

$$\Psi(t) = \begin{cases} 0 & -\infty < t < \infty \\ \text{cubic spline} & \phi < t < \tau \\ \psi & \tau < t < \infty \end{cases}. \quad (14)$$

The peak flux is equal to  $A + \psi$ ,  $\phi$  is the explosion starting time,  $k$  is related to the relative rise and decay times and  $\sigma$  is the light curve width, which gives 5 free parameters. The  $\Psi(t)$  is a tail function which ensures that the flux tends to a finite value for  $t \gg \tau$ , where  $\tau = \phi + k\sigma$  is the peak time. The cubic spline in equation (14) is determined to null the derivative in  $t = \phi$  and  $t = \tau$ . The model is fitted separately for each filter, giving a total of 20 features (21 when we include the host galaxy redshift), for the SDSS *griz* filter system used in the SNPCC. The parameters ranges (which are the same for all bands) are given in table 3.

#### 4.2.2 Karpenka model

The Karpenka model is similar to Newling's, generating a light curve with a peak and a tail which tends to a finite value, but can also describe a situation where a second flux peak can happen. The function is given by

$$F(t) = A [1 + B(t - t_1)^2] \frac{\exp[-(t - t_0)/T_{\text{fall}}]}{1 + \exp[-(t - t_0)/T_{\text{rise}}]}, \quad (15)$$

where  $t$  is taken as the earliest measurement in the r-band light curve. There are 6 free parameters  $\{A, B, t_0, t_1, T_{\text{fall}}, T_{\text{rise}}\}$  for each filter, totalizing 24 free parameters. The ranges of the priors are shown in table 4, which are the same for all bands.

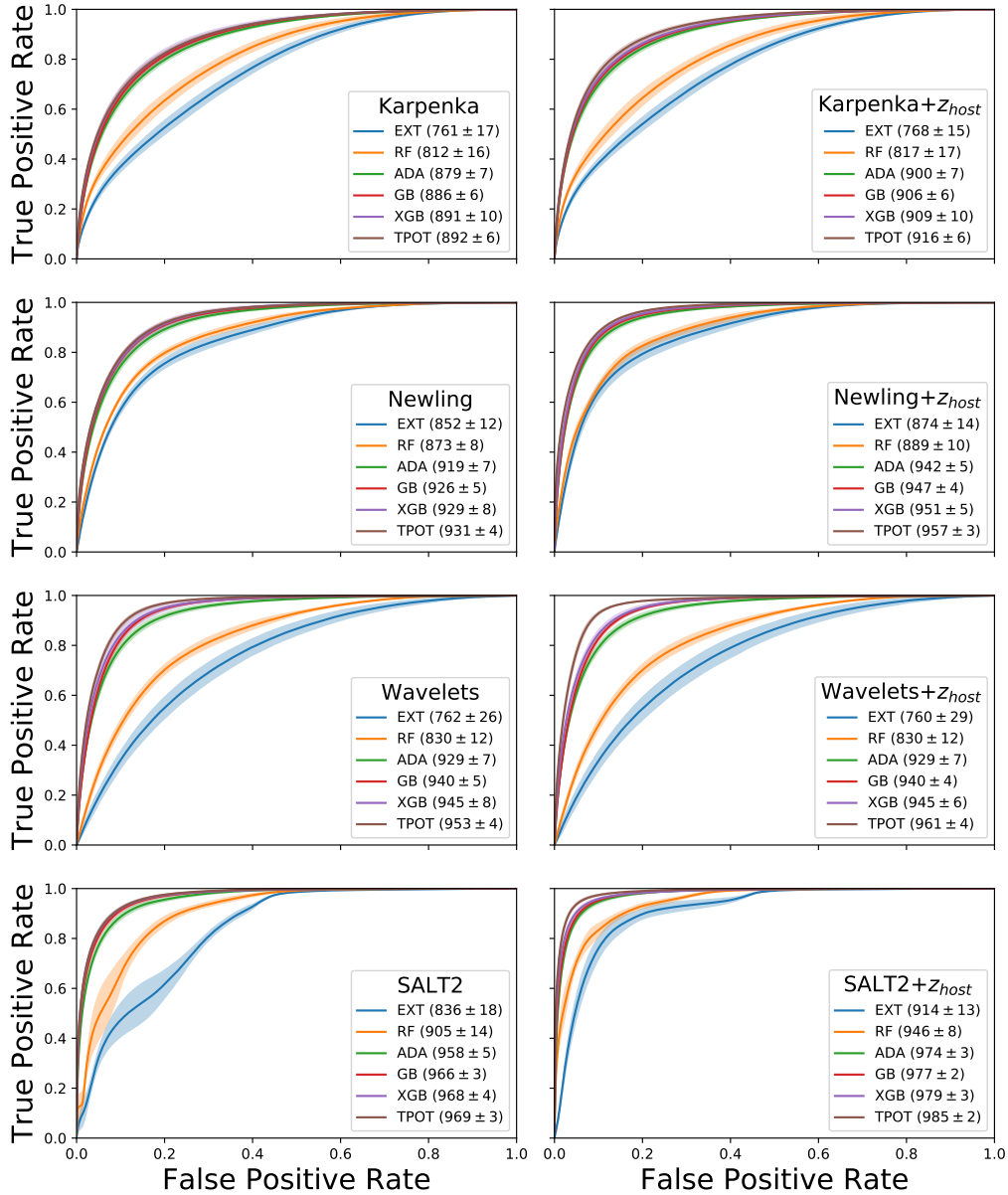


**Figure 4.** ROC curves for each feature set, without (left) and with (right) the host galaxy redshift information, for all ML techniques. The numbers in the legends correspond to the value of  $1000 \times \text{AUC}$  (the area under the curve) for each case.

### 4.3 Wavelet decomposition

The wavelet decomposition is a very useful tool for signal processing and time series analysis, which is the case of supernovae light curves. Following [Lochner et al. \(2016\)](#) we perform the *à trous* wavelet transform, which achieves dyadic scale-invariance, and use the symlet family of wavelets, which are a more symmetric version of the widely used Daubechies family of wavelets, by the implementation `sym2` family provided by the `Pywavelets` library ([pywavelets.readthedocs.io](http://pywavelets.readthedocs.io)). Before using the wavelets we construct an interpolated version of the light curve, for each band, using the Gaussian Random Process provided by the `george` library ([george.readthedocs.io](http://george.readthedocs.io)), where we choose the exponential radial kernel optimized according the procedure described in [george.readthedocs.io/en/latest/tutorials/hyper](http://george.readthedocs.io/en/latest/tutorials/hyper).

We choose 100 points, evenly spaced in the time range of the light curve, for the Gaussian process curve and a two-level wavelet transform, returning 400 coefficients per filter, or 1600 coefficients per object. To avoid redundancy we perform a dimensionality reduction with Principal Components Analysis (PCA) restricting to only the first 20 components, which we use as our feature set.

## 5 RESULTS AND DISCUSSION

### 5.1 Comparison of ML methods with AUC and AP

Let us first analyze the results of the decision trees ensembles. In Figure 4 we compare the ROC curves and the AUC value (given in *per mille* in the plots) for each machine learning model and each set of features. The curves and shaded regions around them are the

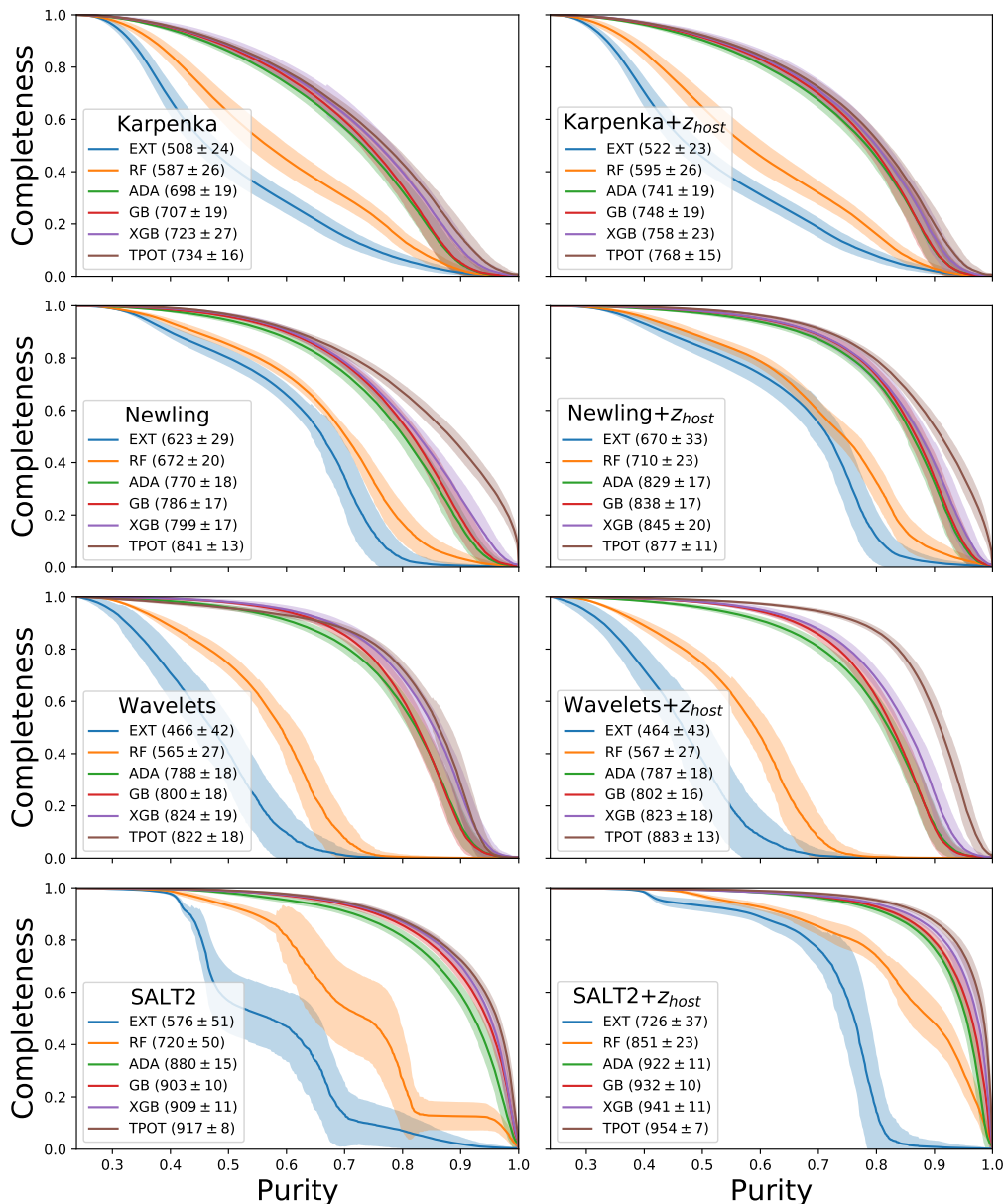


**Figure 5.** Same as Figure 4 for the Completeness-Purity curves. The numbers in the legends correspond here to the value of  $1000 \times \text{AP}$  for each case.

mean and the standard deviation in the catalog set. The AUC values and their uncertainties are likewise obtained this set. As mentioned before, the ideal result is to have an AUC of unity. The first trend we notice in these results is that the boosting methods (**ADA**, **GB**, and **XGB**) reach higher scores than the averaging methods (**EXT** and **RF**) for any set of features. It is also clear that the different boosting methods exhibit very similar performance for all features. TPOT was not able to provide a significant improvement, except for two cases, wavelets and SALT2, both in the case in which we include the host redshift. The *Completeness-Purity* curves are in turn depicted in Figure 5. We note the same difference in average between boosting and averaging methods, although the latter exhibit broader distributions. An interesting feature which is made clear in this score is that even methods with high AP may result in considerably low completeness values for high purities. This happens in general for Wavelets, Karpenka and Newling, but in some

cases using TPOT this issue was alleviated. This means that we may loose a lot of candidates if we need to impose a restrictive purity threshold, which in turn increases the statistical error. For Wavelets (ADA, GB, XGB), for example, if we impose a 90% threshold for the purity, we get a catalog with a completeness of less than 10%. In contrast, for SALT2, we get around 70% of the real positives even when we impose a 90% purity.

Figure 6 compiles the scores for all cases, where we can confirm the ranking between the methods described above, and also compare the features more clearly. The ranking, from low to high score, is: Karpenka, Newling, Wavelets and SALT2. We can also confirm that the introduction of  $z_{\text{host}}$  as feature increases the score as expected and as already reported in L16, except for the case of Wavelets in which it only made any difference when we used TPOT.

Using AP as score we find that the TPOT method was able to increase significantly the scores, as can be seen clearly in Fig-

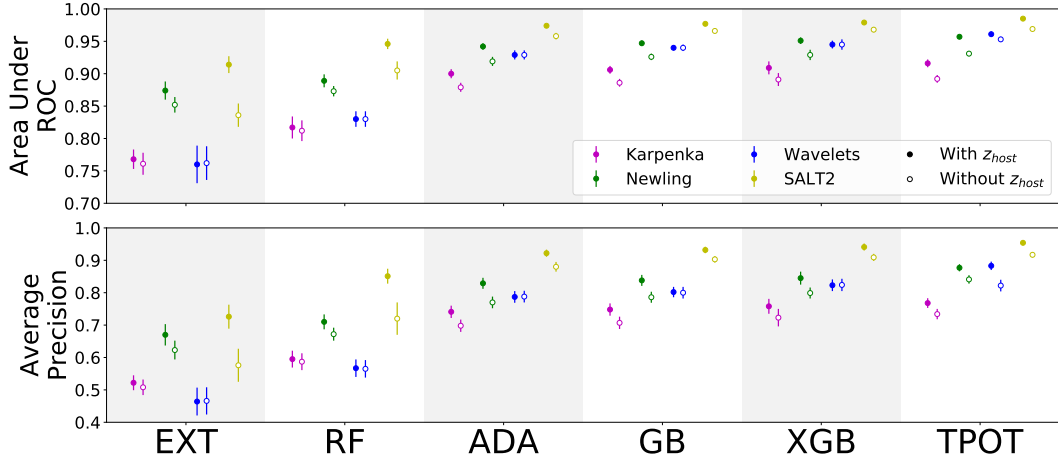


**Figure 6.** Comparison between AUC and AP for each feature set and ML method.

ure 5. It was particularly successful at improving the results using the Newling model and, when  $z_{\text{host}}$  is included, also the Wavelets method. Summarizing the scores for all cases, we find the following.

- Comparing the feature set for different methods we find from best to worst: 1. SALT2; 2. Newling and Wavelets (tied); 3. Karpenka (although when using the averaging ML methods Newling performed better). We stress that since the SALT2 model was used to create the lightcurves the results may be biased toward it. Nevertheless as we discuss below the performance of Newling and Wavelets are still very competitive.
- Comparing the ML methods for given feature sets, from best to worst: 1. TPOT; 2. XGB; 3. GB; 4. ADA; 5. RF; 6. EXT.
- Including  $z_{\text{host}}$  as a new feature: the scores increased in general as expected, except that for Wavelets where it only increased when using TPOT. One should note however that the increase in performance obtained by including the redshift was comparable to the performance difference among ML methods and feature sets. Therefore using TPOT without redshift information still yielded very good results, which is a promising result given that future photometric surveys will only have limited spectroscopic follow-ups.

When we look to the *Completeness-Purity* curves themselves in Figure 5 and not just the AP score, we note some important details. For example, when we compare the curves for Newling and Wavelets, both without including the  $z_{\text{host}}$  as a feature and looking only at the TPOT results we see that if we demand a purity of, say, 95% Newling reaches a completeness of around 30%, significantly larger than that of Wavelets, which lies around 5%. Including  $z_{\text{host}}$  the difference is much smaller but still significant. The final score of Newling is however very similar to the one of Wavelets. This difference in completeness can affect the final analysis. For instance when we compute statistics on cosmological distances, as we do below. From now on we focus the analysis only on the catalogs generated by the TPOT pipelines, optimized by including  $z_{\text{host}}$  as a feature.

## 5.2 Analysis of the Bias-Variance tradeoff

Figure 7 shows the evolution of bias for each feature set, for three purity cuts (70%, 80% and 90%) for the different feature sets in comparison to both a completely random classifier and a perfect classifier (which always returns a catalog of  $\mathcal{P} = \mathcal{L} = 1$ ). A common feature for all cases is that the bias is low for intermediate redshifts ( $0.4 < z < 0.9$ ), and high for both low and high redshifts ( $z < 0.4$ , and  $z > 0.9$ ). We can also see that the bias values in general decreases as the purity increases, in contrast to the error bars which increase due to the loss in the number of classified objects. The balance is set by the Bias-Variance tradeoff, described in Section 3.1. Interestingly though, for high purities the bias becomes negative, so the tradeoff actually penalises very high purities not only due to the low completeness, but also due to the higher absolute values of the bias. One would naïvely expect the bias to be a monotonically function of the purity, but this *a priori* unexpected behavior of the bias is explained below.

In Figure 8 we depict how each SN type contributes to the magnitudes by showing the bin counts of absolute magnitudes ( $M_B = m_B^* - \mu_{\text{fid}}(z_{\text{sim}})$ ) for four different purity values (70%, 80%, 90% and 95%). We depict the particular cases of SALT2 and Newling, but the overall trend is similar in all cases: the type II SN are the first to be excluded as we increase the purity threshold, followed by the types Ibc. This means that the algorithms are more efficient at distinguishing between types I and II than between Ia and CC. Since types II and Ibc are on opposing  $M_B$  extremes, and since type IIs have a larger magnitude difference, as the purity threshold increases the magnitude bias due to CC SNe changes sign, instead of monotonically approaching zero. Interestingly, in the case of SALT2 and Wavelets, for large purity thresholds our classifier ends up mis-classifying mostly the CC SNe which have similar magnitudes to the ones of type Ia. This means that for these feature sets the CC contaminants for high purity thresholds may end up mimicking the type Ia standard candles. This peculiar behavior of the bias is fundamentally due to the ML trying to reduce the 8 classes of SN to a simple binary classification: Ia versus CC.

The dependence of the RMSE with the purity is shown in Figure 9. The green line is the contribution due to the variance, the blue one is the contribution due to the bias and the red thick line is the total RMSE. The dotted gray lines are the RMSE computed in each redshift bin. Note that, close to the minimum, the variance is al-

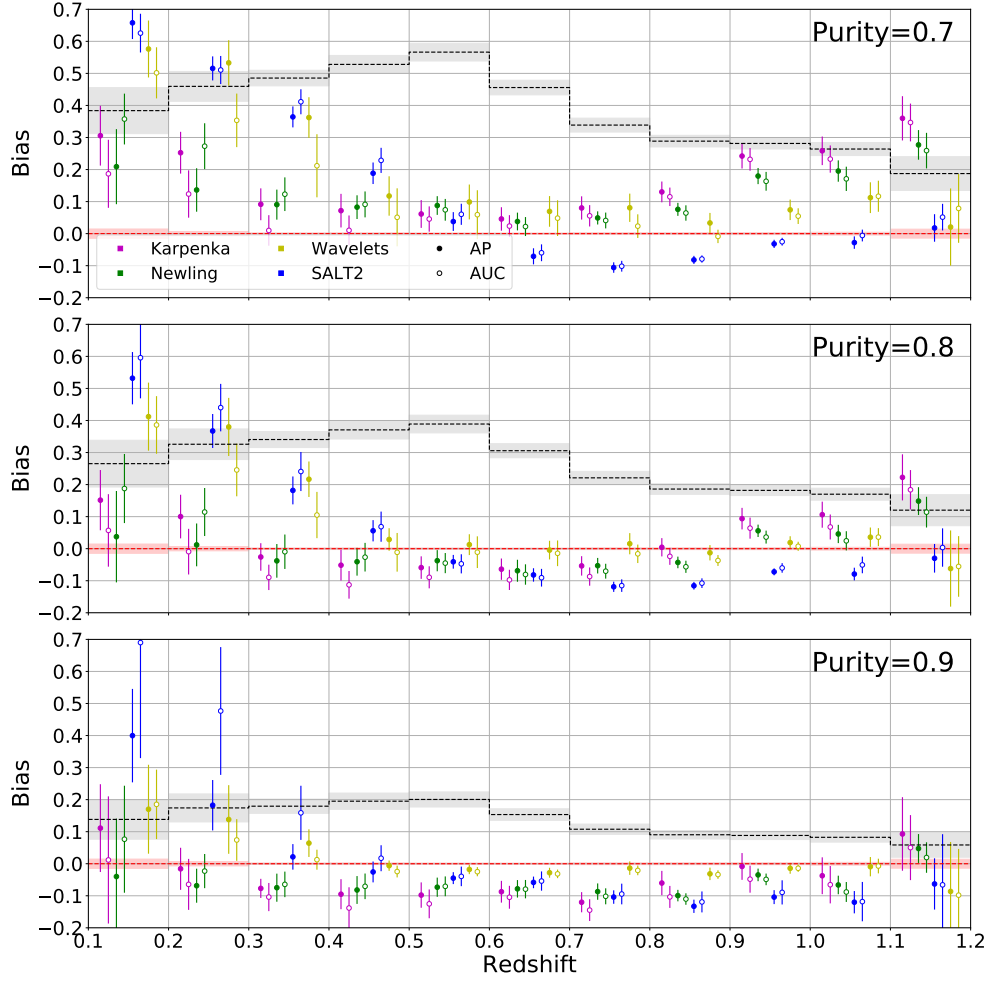


**Figure 7.** Evolution of bias with the redshift for three values of purity. Data points are slightly displaced left and right for clarity, but they are all for the bin centers. The red dashed line and shaded region correspond to values and standard deviation for a perfect classifier, type Ia supernovae only (TP+FN). The black dashed line and gray region represents a completely random classifier. Note that for high purities the bias becomes negative in many cases [see text].

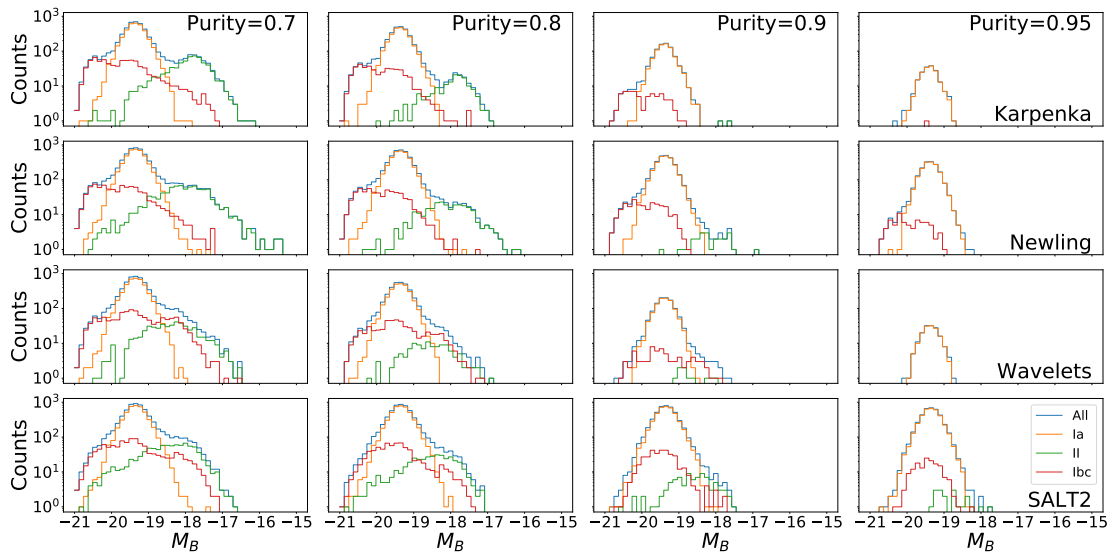


**Figure 8.** Supernovae count by bins of absolute magnitude with AUC as the optimization score. Since the classifier performs best against type II SN than types Ibc, for very high purities only the latter contaminants remain, and since type II and Ibc are on opposite magnitude extremes, the bias changes sign.

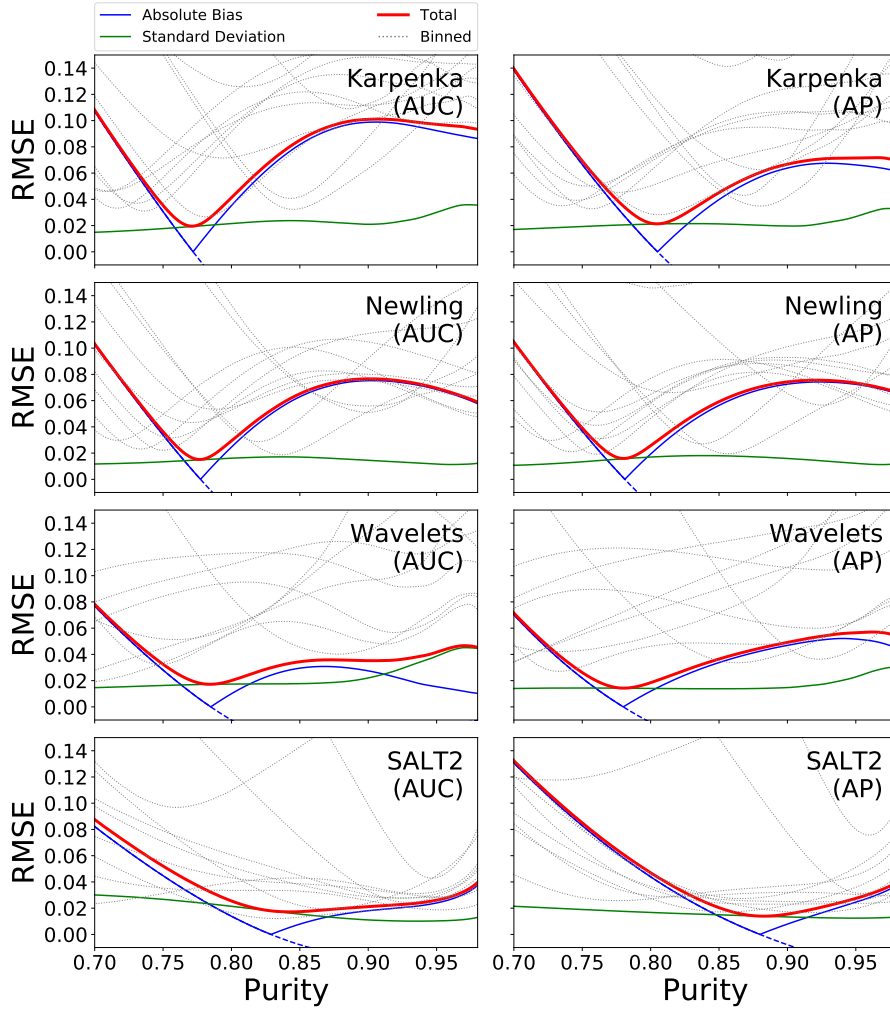


**Figure 9.** Evolution of RMSE with the Purity, using AUC (left) and AP (right) as scores. The green line is the contribution due to the variance, the blue line is the contribution due to the bias and the red thick line is the total RMSE. The dotted gray lines are the RMSE computed in each redshift bin.

most constant while the bias changes sign. I.e. the RMSE minimum value is determined by the variance while the minimum purity, by the bias.

We use this dependence to choose what is the best probability threshold, once it is univocally determined by the purity. The simplest choice is the probability which minimizes the total MSE, a constant purity cut, however we may get very high values of RMSE in some redshift bins. Perhaps, the best way of selecting the sample is to choose the purity values that minimize the RMSE in each redshift bin, which we dub binned purity. I.e. we construct a new catalog which each bin is taken from other catalog which the purity minimizes the MSE of that bin. To avail which is the best method we check how much each choice affect the final cosmological constraints. In this context the aim is find the model which fits the data, i.e. minimizes the follow quantity

$$\begin{aligned} \chi^2 &= [\mu - \mu(z)] \cdot C^{-1} \cdot [\mu - \mu(z)]^T \\ &= \sum_{b=1}^{N=11} \sum_{b'=1}^{N=11} [\bar{\mu}_b - \mu(\bar{z}_b)] C_{bb'}^{-1} [\bar{\mu}_{b'} - \mu(\bar{z}_{b'})], \quad (16) \end{aligned}$$

where  $\mu = (\bar{\mu}_1, \bar{\mu}_2, \dots, \bar{\mu}_{11})$ ,  $z = (\bar{z}_1, \bar{z}_2, \dots, \bar{z}_{11})$ , and  $C$  is the covariance matrix. Defining the error as  $\sigma_b^2 = \text{MSE}_b = \langle \Delta\bar{\mu}_b \Delta\bar{\mu}_b \rangle$ , we generalize it for correlated bins as  $C_{bb'} = \langle \Delta\bar{\mu}_b \Delta\bar{\mu}_{b'} \rangle$  so the covari-

ance for a single catalog is  $C_{bb'} = \Delta\bar{\mu}_b \Delta\bar{\mu}_{b'}$ , therefore

$$C_{bb'} = \left( \frac{\text{Var}_b}{N_{SN}^b} \right) \delta_{bb'} + b_b b_{b'}. \quad (17)$$

In order to assess how the different ML techniques behaved in a cosmological analysis, we fitted a flat  $\Lambda$ CDM model and obtained the constraints on the current matter density parameter  $\Omega_{m0}$ , marginalizing over the overall distance scale which is a combination of the unknown SN absolute magnitude and the Hubble parameter  $H_0$ . The constraints on  $\Omega_{m0}$  are shown in Figure 10, where we compare the selection criteria (constant or binned purity thresholds) and the different ML feature sets. We also indicate the result for a perfect classifier in red and the fiducial value used in SNPCC ( $\Omega_{m0} = 0.3$ ) in black. All of them deviates very little from wither the perfect classifier or the fiducial (less than half- $\sigma$ ).

If we assume that all Type Ia supernovae contribute with the same amount of information, the effective statistical error on a cosmological parameter should scale as  $\sigma_{Ia} = \sigma_1 / \sqrt{N_{Ia}}$ , where  $\sigma_1$  is the contribution of each Ia supernovae. We extrapolate on this idea to define  $N_{Ia}^{\text{eff}}$ , the effective number of SNIa in a final photometric classified catalog, as  $N_{Ia}^{\text{eff}} = (\sigma_{Ia} / \sigma)^2 N_{Ia}$ . We likewise define the

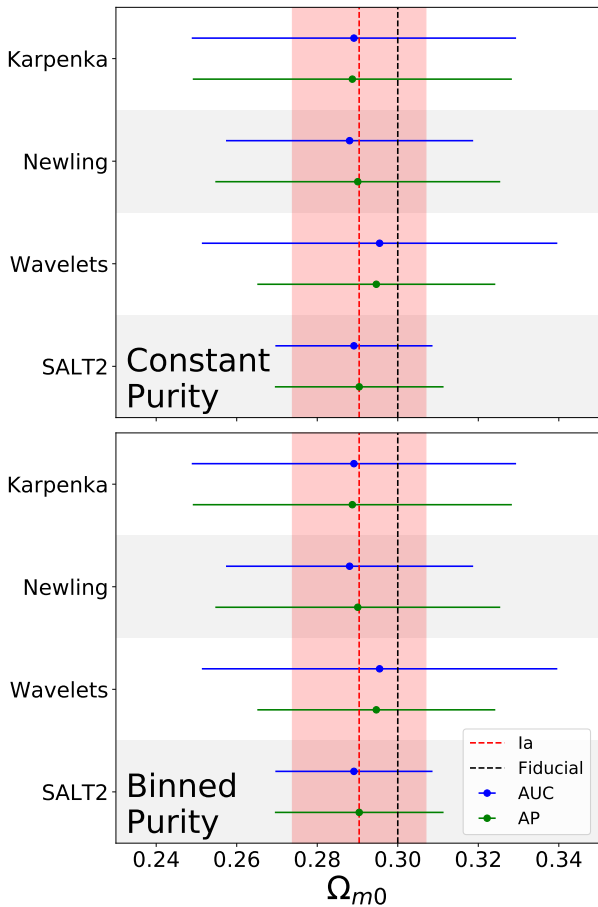


**Figure 10.**  $\Omega_{m0}$  constraints obtained for each feature set when using a constant purity (top) and choosing purity per redshift bin (bottom).

*effective completeness*  $\mathcal{C}^{\text{eff}}$  as

$$\mathcal{C}^{\text{eff}} \equiv N_{\text{Ia}}^{\text{eff}} / N_{\text{Ia}}. \quad (18)$$

This quantity is computed in table 5 for different methods. SALT2 preserves up to 75% of the information in the best scenarios, Newling and Wavelets around 30 – 35% and Karpenka only 20%. This means that even if one drops SALT2 since our SNe may be biased toward it, one still retains around a third of all the information in the SNeIa data without spectroscopy.

To check the validity of our fit we also computed the value of the so-called  $R^2$  score (or coefficient of determination<sup>8</sup>). In all cases  $R^2$  was found to be very close to unity ( $|1 - R^2| \sim 10^{-5}$ ).

## 6 CONCLUSIONS

In this work we used simulated data from the Supernova Photometric Classification Challenge (SNPCC) to assess the performance of a series of machine learning methods applied to the problem of supernova classification. We considered some flavors of ensemble Decision Trees provided by `scikit-learn`: Adaptive Boosting (**ADA**), RandomForest (**RF**), ExtraTrees (**EXT**), Gradient Boosting (**GB**), and the Extreme Gradient Boosting (**XGB**) provided by

<sup>8</sup> [https://scikit-learn.org/stable/modules/generated/sklearn.metrics.r2\\_score.html](https://scikit-learn.org/stable/modules/generated/sklearn.metrics.r2_score.html)

	Constant Purity		Binned Purity	
	AUC	AP	AUC	AP
Karpenka	(16 ± 5)%	(20 ± 4)%	(19 ± 6)%	(19 ± 5)%
Newling	(30 ± 4)%	(23 ± 6)%	(32 ± 9)%	(24 ± 7)%
Wavelets	(22 ± 4)%	(22 ± 4)%	(16 ± 8)%	(36 ± 13)%
SALT2	(54 ± 17)%	(48 ± 14)%	(75 ± 15)%	(66 ± 15)%

**Table 5.** The *effective completeness* of each method. This quantifies how much information is preserved after the photometric classification.

the `XGBoost` library. We also tested an alternative metric to characterize the performance of the classifier, the AP, and compared the results with the AUC used in L16. In addition we performed an automated machine learning training by using TPOT, in order to find the best pipelines for each feature set. Regarding the features, we four different models, Karpenka, Newling, wavelets and SALT2. We then explored how a ML-classified SN catalog performs in cosmological parameter estimation, quantifying the degradation due to the imperfect completeness and purity of the resulting catalogs.

We conclude that, among the features, the SALT2 gave the best overall results. Considering that this model was used in the generation of the simulated data, it is not clear to what extent the data itself was possibly biased toward this model, and this question certainly deserve to be investigated in the future. If one thus neglects the SALT2 feature set, both Wavelets and Newling models performed similarly. The Karpenka model performed consistently the worst.

Regarding the scores, we found that the AP was more effective to discriminate between the ML methods as opposed to the AUC, which gave essentially the same results for all boosting methods and TPOT. The boosting methods were considerably better than the averaging ones for both metrics. We showed that, considering the AP score, TPOT was capable to provide a pipeline more efficient than the boosting methods tested in this work.

We tested two ways for selecting the purity probability threshold: either imposing a constant purity for the whole sample or choosing different purity levels in each redshift bin in order to optimize the MSE. We found that both choices yielded good results for a flat  $\Lambda$ CDM model. Employing the Bias-Variance tradeoff we were able to consistently produce photometric classified catalogs that were within half- $\sigma$  of the fiducial model and of a perfect classifier.

We also computed how much cosmological information was preserved after classification using each feature set with the best ML method, TPOT. We found out that SALT2 is able to preserve up to 75% of the information, while the other second-best alternatives, based on either the Newling model or Wavelet decomposition, around 30 – 35%. This is a very important quantity (it can be interpreted as an effective completeness), as future surveys like LSST will have a huge number of observed SN, but the majority without any spectra. Table 5 summarizes how much information each fit preserves, compared to a perfect classifier.

It is important to stress that an analysis based on the Bias-Variance Trade-off assumes that the bias cannot be modeled. In fact, as CC SNe lightcurves become better understood it may become possible to predict their impact on the distance estimation and thus mitigate the bias they introduce. This would allow even better performance of the ML photometric classification techniques.

Automated machine learning training techniques are an interesting and very efficient way of attacking the problem of supernova

photometric classification for cosmological uses, and we recommend their application in future ML studies in astronomy.

## ACKNOWLEDGEMENTS

This work made use of the CHE cluster, managed and funded by COSMO/CBPF/MCTI, with financial support from FINEP and FAPERJ. We would like to thank Michelle Lochner for sharing her code, Martin Makler for access to the CHE cluster and Luca Amendola and Luciano Casarini for useful suggestions. MVS is supported by the Brazilian research agency FAPERJ. MQ is also supported by FAPERJ and by the Brazilian research agency CNPq.

## REFERENCES

Abbott T., et al., 2016, MNRAS, 460, 1270, [1601.00329](#)  
 Abdalla F. B., Banerji M., Lahav O., Rashkov V., 2011, MNRAS, 417, 1891, [0812.3831](#)  
 Abell P. A., et al., 2009, [0912.0201](#)  
 Bazin G., et al., 2009, A&A, 499, 653, [0904.1066](#)  
 Bellm E. C., 2014, Proceedings of the Third Hot-Wiring the Transient Universe Workshop, 1, 1, [astro-ph/1410.8185](#)  
 Betoule M., et al., 2014, Astron.Astrophys., 568, A22, [1401.4064](#)  
 Birrer S., et al., 2019, MNRAS, 484, 4726, [1809.01274](#)  
 Bonvin V., et al., 2017, MNRAS, 465, 4914, [1607.01790](#)  
 Burns C. R., et al., 2018, ApJ, 869, 56, [1809.06381](#)  
 Castro T., Quartin M., 2014, MNRAS, 443, L6, [1403.0293](#)  
 Castro T., Quartin M., Benitez-Herrera S., 2016, Phys. Dark Univ., 13, 66, [1511.08695](#)  
 Charnock T., Moss A., 2017, ApJ, 837, L28, [1606.07442](#)  
 Colin J., Mohayaee R., Sarkar S., Shafieloo A., 2011, MNRAS, 414, 264, [1011.6292](#)  
 Dahlen T., et al., 2013, ApJ, 775, 93, [1308.5353](#)  
 Dilday B., et al., 2008, ApJ, 682, 262, [0801.3297](#)  
 Fawcett T., 2004, Machine Learning, 31, 1  
 Garcia K., Quartin M., Siffert B. B., 2019, [1905.00746](#)  
 Gomes Z., Jarvis M. J., Almosallam I. A., Roberts S. J., 2018, MNRAS, 475, 331, [1712.02256](#)  
 Gordon C., Land K., Slosar A., 2007, Physical Review Letters, 99, 081301, [0705.1718](#), [ADS](#)  
 Guy J., et al., 2007, A&A, 466, 11, [astro-ph/0701828](#)  
 Howlett C., Robotham A. S. G., Lagos C. D. P., Kim A. G., 2017, ApJ, 847, 128, [1708.08236](#)  
 Huber S., et al., 2019, [1903.00510](#)  
 Ishida E. E. O., 2019, Nature Astronomy, 3, 680  
 Ishida E. E. O., de Souza R. S., 2013, MNRAS, 430, 509, [1201.6676](#)  
 Jha S., Riess A. G., Kirshner R. P., 2007, Astrophys.J., 659, 122, [astro-ph/0612666](#)  
 Jones D. O., et al., 2018, ApJ, 857, 51, [1710.00846](#)  
 Karpenka N. V., Feroz F., Hobson M. P., 2013, MNRAS, 429, 1278, [1208.1264](#)  
 Kessler R., Conley A., Jha S., Kuhlmann S., 2010b, [1001.5210](#)  
 Kessler R., et al., 2009, ApJS, 185, 32, [0908.4274](#)  
 Kessler R., et al., 2010a, Publ. Astron. Soc. Pac., 122, 1415, [1008.1024](#)  
 Kgoadi R., Engelbrecht C., Whittingham I., Tkachenko A., 2019, Preprint, 000, 1, [1906.06628](#)  
 Koivisto T. S., Mota D. F., Quartin M., Zlosnik T. G., 2011, Phys. Rev., D83, 023509, [1006.3321](#)  
 Kunz M., Bassett B. A., Hlozek R., 2007, Phys. Rev., D75, 103508, [astro-ph/0611004](#)  
 Lochner M., McEwen J. D., Peiris H. V., Lahav O., Winter M. K., 2016, ApJS, 225, 31, [1603.00882](#)  
 Macaulay E., Davis T. M., Scovacricchi D., Bacon D., Collett T. E., Nichol R. C., 2017, MNRAS, 467, 259, [1607.03966](#)  
 Malz A. I., et al., 2018, [1809.11145](#)

Markel J., Bayless A. J., 2019, [1907.00088](#)  
 Moss A., 2018, [1810.06441](#)  
 Newling J., Bassett B., Hlozek R., Kunz M., Smith M., Varughese M., 2012, MNRAS, 421, 913, [1110.6178](#)  
 Newling J., Varughese M., Bassett B. A., Campbell H., Hlozek R., Kunz M., Lampeitl H., Martin B., Nichol R., Parkinson D., Smith M., 2010, [1010.1005](#)  
 Oguri M., Marshall P. J., 2010, MNRAS, 405, 2579, [1001.2037](#)  
 Pedregosa F., et al., 2011, J. Machine Learning Res., 12, 2825, [1201.0490](#)  
 Quartin M., Marra V., Amendola L., 2014, Phys.Rev., D89, 023009, [1307.1155](#)  
 Riess A. G., et al., 2016, ApJ, 826, 56, [1604.01424](#)  
 Sadeh I., Abdalla F. B., Lahav O., 2016, Publ. Astron. Soc. Pac., 128, 104502, [1507.00490](#)  
 Sako M., et al., 2008, AJ, 135, 348, [0708.2750](#)  
 Sako M., et al., 2018, Publ. Astron. Soc. Pac., 130, 064002, [1401.3317](#)  
 Scolnic D. M., et al., 2018, ApJ, 859, 101, [1710.00845](#)  
 Soltis J., Farahi A., Huterer D., Liberato C. M., 2019, Phys. Rev. Lett., 122, 091301, [1902.07189](#)  
 Swets J. A., Dawes R. M., Monahan J., 2000, Scientific American, 283, 82, [ADS](#)  
 Villar V. A., et al., 2019, [1905.07422](#)

## APPENDIX A: TPOT PIPELINES

Here we provide the best pipelines obtained with TPOT for each feature set and optimization criterion. They are ready to use as argument of the function `sklearn.pipeline.make_pipeline`.

- Karpenka, optimized by AP:

```
make_union(
    make_pipeline(
        PolynomialFeatures(
            degree=2, include_bias=False,
            interaction_only=False
        ),
        SelectFwe(
            score_func=f_classif,
            alpha=0.033
        )
    ),
    GradientBoostingClassifier(
        learning_rate=0.1, max_depth=9,
        max_features=0.25, min_samples_leaf=8,
        min_samples_split=12, n_estimators=100,
        subsample=0.9
    )
)
```

- Karpenka, optimized by AUC:

```
GradientBoostingClassifier(
    learning_rate=0.1, max_depth=8,
    max_features=0.85, min_samples_leaf=4,
    min_samples_split=11, n_estimators=100,
    subsample=0.9
)
```

- Karpenka +  $z_{\text{host}}$ , optimized by AP:

```
ZeroCount(),
GradientBoostingClassifier(
    learning_rate=0.1, max_depth=10,
    max_features=1.0, min_samples_leaf=8,
```

```

n_estimators=100, subsample=0.75
)
• Karpenka +zhost, optimized by AUC:
make_union(
    FunctionTransformer(copy),
    make_pipeline(
        VarianceThreshold(threshold=0.2),
        FastICA(tol=0.0)
    )
),
XGBClassifier(
    learning_rate=0.1, max_depth=9,
    min_child_weight=2, n_estimators=100,
    nthread=1, subsample=0.8
)
• Newling, optimized by AP:
make_union(
    make_union(
        FunctionTransformer(copy),
        FunctionTransformer(copy)
    ),
    make_pipeline(
        Normalizer(norm="l2"),
        RFE(estimator=ExtraTreesClassifier(
            criterion="entropy",
            max_features=0.75,
            n_estimators=100
        ), step=0.15
    ),
    RFE(
        estimator=ExtraTreesClassifier(
            criterion="gini",
            max_features=0.05,
            n_estimators=100
        ),
        step=0.95
    ),
    FastICA(tol=0.55),
    RBFSampler(gamma=0.8),
    RFE(
        estimator=ExtraTreesClassifier(
            criterion="entropy",
            max_features=0.15,
            n_estimators=100
        ),
        step=0.4
    )
),
ExtraTreesClassifier(
    bootstrap=False, criterion="entropy",
    max_features=0.95, min_samples_leaf=2,
    min_samples_split=5, n_estimators=100
)
• Newling, optimized by AUC:
Normalizer(norm="l2"),
StackingEstimator(
    estimator=LinearSVC(
        C=5.0, dual=False,

```

```

        loss="squared_hinge",
        penalty="l1", tol=0.01
    )
),
GradientBoostingClassifier(
    learning_rate=0.1, max_depth=9,
    max_features=0.85, min_samples_leaf=14,
    min_samples_split=9, n_estimators=100,
    subsample=0.85
)
• Newling +zhost, optimized by AP:
make_union(
    FunctionTransformer(copy),
    FunctionTransformer(copy)
),
MinMaxScaler(),
RFE(
    estimator=ExtraTreesClassifier(
        criterion="entropy",
        max_features=0.3,
        n_estimators=100
    ),
    step=1.0
),
PolynomialFeatures(
    degree=2, include_bias=False,
    interaction_only=False
),
SelectFwe(
    score_func=f_classif, alpha=0.004
),
ExtraTreesClassifier(
    bootstrap=False, criterion="entropy",
    max_features=0.25, min_samples_leaf=2,
    min_samples_split=3, n_estimators=100
)
• Newling +zhost, optimized by AUC:
RFE(
    estimator=ExtraTreesClassifier(
        criterion="entropy",
        max_features=0.75,
        n_estimators=100
    ),
    step=0.2
),
ExtraTreesClassifier(
    bootstrap=False,
    criterion="gini",
    max_features=0.95,
    min_samples_leaf=1,
    min_samples_split=2,
    n_estimators=100
)
• SALT2, optimized by AP:
StackingEstimator(
    estimator=LinearSVC(
        C=20.0, dual=False,
        loss="squared_hinge",
        penalty="l2", tol=0.0001

```

```

    )
),
StackingEstimator(
    estimator=LinearSVC(
        C=10.0, dual=True,
        loss="squared_hinge",
        penalty="l2", tol=0.1
    )
),
ZeroCount(),
RandomForestClassifier(
    bootstrap=False, criterion="entropy",
    max_features=0.35, min_samples_leaf=3,
    min_samples_split=9, n_estimators=100
)
• SALT2, optimized by AUC:
make_union(
    FunctionTransformer(copy),
    make_union(
        make_pipeline(
            RBFSampler(gamma=0.35),
            Normalizer(norm="l1")
        ),
        FunctionTransformer(copy)
    ),
    FunctionTransformer(copy)
),
RandomForestClassifier(
    bootstrap=False, criterion="entropy",
    max_features=0.2, min_samples_leaf=2,
    min_samples_split=7, n_estimators=100
)
• SALT2 + zhost, optimized by AP:
make_union(
    FunctionTransformer(copy),
    make_union(
        make_pipeline(
            FastICA(tol=0.65),
            FastICA(tol=0.0),
            ZeroCount()
        ),
        FunctionTransformer(copy)
    )
),
RandomForestClassifier(
    bootstrap=False, criterion="entropy",
    max_features=0.4, min_samples_leaf=1,
    min_samples_split=4, n_estimators=100
)
• SALT2 + zhost, optimized by AUC:
make_union(
    FunctionTransformer(copy),
    FastICA(tol=0.05)
),
StackingEstimator(
    estimator=LogisticRegression(
        C=0.5, dual=False,

```

```

        penalty="l1"
    )
),
RandomForestClassifier(
    bootstrap=True, criterion="entropy",
    max_features=0.2, min_samples_leaf=1,
    min_samples_split=2, n_estimators=100
)
• Wavelets, optimized by AP:
PolynomialFeatures(
    degree=2, include_bias=False,
    interaction_only=False
),
StackingEstimator(
    estimator=ExtraTreesClassifier(
        bootstrap=True,
        criterion="gini",
        max_features=0.25,
        min_samples_leaf=7,
        min_samples_split=17,
        n_estimators=100
    )
),
StackingEstimator(
    estimator=LogisticRegression(
        C=1.0, dual=False, penalty="l1"
    )
),
MaxAbsScaler(),
RFE(
    estimator=ExtraTreesClassifier(
        criterion="entropy",
        max_features=0.75,
        n_estimators=100
    ),
    step=0.1
),
StackingEstimator(estimator=GaussianNB()),
MinMaxScaler(),
XGBClassifier(
    learning_rate=0.1, max_depth=4,
    min_child_weight=1, n_estimators=100,
    nthread=1, subsample=0.6
)
• Wavelets, optimized by AUC:
make_union(
    make_pipeline(
        Normalizer(norm="l2"),
        FastICA(tol=0.7)
    ),
    FunctionTransformer(copy)
),
StackingEstimator(
    estimator=ExtraTreesClassifier(
        bootstrap=False,
        criterion="entropy",
        max_features=0.9,
        min_samples_leaf=3,
        min_samples_split=6,
        n_estimators=100
    )

```

```

    )
),
RobustScaler(),
ZeroCount(),
LogisticRegression(
    C=0.5, dual=True,
    penalty="l2"
)

```

- Wavelets +  $z_{\text{host}}$ , optimized by AP:

```

make_union(
    Nystroem(
        gamma=0.15, kernel="linear",
        n_components=10
    ),
    StackingEstimator(
        estimator=make_pipeline(
            StackingEstimator(
                estimator=LogisticRegression(
                    C=25.0,
                    dual=False,
                    penalty="l1"
                )
            ),
            PolynomialFeatures(
                degree=2,
                include_bias=False,
                interaction_only=False
            ),
            LogisticRegression(
                C=0.001, dual=False,
                penalty="l2"
            )
        )
    )
),
GradientBoostingClassifier(
    learning_rate=0.1, max_depth=8,
    max_features=0.8, min_samples_leaf=4,
    min_samples_split=10, n_estimators=100,
    subsample=0.9
)

```

- Wavelets +  $z_{\text{host}}$ , optimized by AUC:

```

make_union(
    StackingEstimator(
        estimator=KNeighborsClassifier(
            n_neighbors=21, p=1,
            weights="uniform"
        )
    ),
    StackingEstimator(
        estimator=make_pipeline(
            RBFSampler(gamma=0.1),
            ExtraTreesClassifier(
                bootstrap=False,
                criterion="entropy",
                max_features=0.25,
                min_samples_leaf=18,
                min_samples_split=7,
                n_estimators=100
            )
        )
    )
)

```

```

    )
),
MaxAbsScaler(),
GradientBoostingClassifier(
    learning_rate=0.1, max_depth=7,
    max_features=0.9, min_samples_leaf=12,
    min_samples_split=9, n_estimators=100,
    subsample=0.85
)

```

This paper has been typeset from a  $\text{\TeX}/\text{\LaTeX}$  file prepared by the author.